

# Dynamic Performance Analysis, Optimization, and Verification of DC Auto-Transformer System With Rail Potential and Stray Current Emulator

Miao Wang<sup>ID</sup>, Student Member, IEEE, Xiaofeng Yang<sup>ID</sup>, Senior Member, IEEE, Menghan Ni<sup>ID</sup>, Shixiang Li<sup>ID</sup>, Huikang Wang<sup>ID</sup>, and Trillion Q. Zheng<sup>ID</sup>, Senior Member, IEEE

**Abstract**—DC auto-transformer (DCAT) traction power supply system has been studied to suppress the rail potential and stray current for urban rail transit (URT), which generally takes the constant train load to simplify the analysis. However, in practice, the train is a non-linear load with frequent accelerating and braking, which leads to the rail potential and stray current changing with different train operating conditions. Therefore, the dynamic performance analysis and optimization of DCAT system are discussed in this article. The rail potential and stray current dynamic emulator (RSDE) for DCAT system verification is proposed because it is difficult to test the DCAT system directly in the actual URT. Based on the configurations and operation principles of both DCAT system and RSDE, the comparisons between DCAT system and the existing system on the rail potential and stray current are discussed. Meanwhile, considering the train dynamic performance, define the dynamic performance index (DPI) to evaluate the effects of the DCAT system on the rail potential and stray current mitigation and optimize the DCAT system with DPI. Finally, the correctness and effectiveness of DCAT system on the rail potential and stray current mitigation are validated by the simulation results and experimental verification.

**Index Terms**—DC auto-transformer (DCAT), dynamic performance, rail potential, stray current, urban rail transit (URT).

## I. INTRODUCTION

NOWADAYS, with rapid development of urban rail transit (URT) in the world, the rail potential and stray current issues attract more attention gradually [1], [2]. URT generally adopts dc traction power supply as shown in Fig. 1, and the running rails act as the return path of traction current to the negative cubicle of traction substation (TS) [3], [4]. However, the rails are not totally isolated from the earth. A part of current leaks from the rails to the earth and becomes stray current, which causes the serious interference on URT signaling equipment and electrochemical corruptions on the rail, metallic pipelines, and underground structures [5]–[8].

Manuscript received April 16, 2021; revised June 21, 2021; accepted July 22, 2021. Date of publication August 3, 2021; date of current version March 22, 2022. This work was supported by the Key Program of National Natural Science Foundation of China under Grant 51737001. (*Corresponding authors: Xiaofeng Yang; Trillion Q. Zheng.*)

The authors are with the School of Electrical Engineering, Beijing Jiaotong University, Beijing 100044, China (e-mail: wangmiao@bjtu.edu.cn; xfyang@bjtu.edu.cn; 18121481@bjtu.edu.cn; 19121452@bjtu.edu.cn; 18121501@bjtu.edu.cn; tqzheng@bjtu.edu.cn).

Digital Object Identifier 10.1109/TTE.2021.3102424

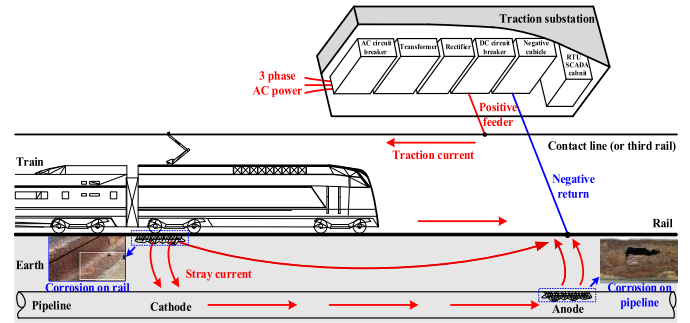


Fig. 1. Stray current issue of dc traction power supply.

Meanwhile, there is a significant potential difference between the rails and earth, which is called rail potential. Higher rail potential endangers the personal safety and normal operation of URT [9], [10].

For the rail potential and stray current mitigation, many measures have been adopted in URT. The typical mitigation measures include: optimizing TS power supply, strengthening the rail-to-earth insulation, setting the stray current collection mat, adopting the cathodic protection [11]–[14], and so on. However, these measures are mainly adopted in URT construction stage with high costs, while the performances deteriorate over time. And it is difficult to renovate for the long-running URT with serious stray current leakage. Meanwhile, URT generally installs the over voltage protection device (OVPD) at TS [15], which connects the rails to earth directly once the rail potential exceeds its threshold value. However, the stray current of URT increases significantly when OVPD is activated [16], [17], and OVPD may be activated frequently during rush hour. Therefore, new technology on the rail potential and stray current mitigation is urgently required because of the existing measures' limitation. Considering that the source of rail potential and stray current issues is the rail-retumed current [18], these issues may be solved fundamentally if the rail current is transferred to other lines with the power electronic technology.

Many power-electronic-technology-based traction power supply systems for URT have been studied in recent years. Medium-voltage dc three-wire supply system is presented in [19], which transfers parts of rail current to the additional feed line through dc chopper, but the rest current still flows

back to TS through the running rail. Fotouhi *et al.* [20] presented dc booster circuit for the dc traction power supply system, which may transfer the total rail current to the return current line. However, each dc booster consists of two dc inductors and 11 switches, which leads to complex control and high cost. Moreover, the negative resistance converter (NRC) traction power system is presented in [21] and [22]. Here, NRC and switch units provide zero-resistance loops to shorten the return path of rail current, and the rail current may be transferred to the return line completely. NRC has fewer components (i.e., one dc inductor and four switches) compared with dc booster in [20], but the NRC system requires multiple voltage sensors and real-time train position to ensure that NRC and multiple switch units operate accurately.

Thus, the dc auto-transformer (DCAT) traction power supply system has been introduced for the rail potential and stray current mitigation [23]–[25]. Compared with other power-electronic-technology-based systems, the DCAT system transfers the total rail current with simple topology. The rail current is automatically transferred through both the nearest left and right DCATs without real-time train position detection. In [23], the rail potential and stray current of DCAT system under different grounding schemes were discussed. However, a previous DCAT system research generally adopts the constant train load to simplify the analysis. But in practice, as a non-linear load, the train position and current change with different operating conditions, such as traction, coasting, and braking [26]–[29]. The rail potential and stray current also change with different train operating conditions. Then the rail potential and stray current of the actual URT are significantly different from those in the simplified analysis. Therefore, it is necessary to study the dynamic performance analysis and optimization of the DCAT system on the rail potential and stray current mitigation. Moreover, to emulate the rail potential and stray current behavior of URT, Ibrahim *et al.* [30] presented the rail potential and stray current dynamic emulator (RSDE) for realizing the train position and current change. But RSDE in [30] is not suitable for the DCAT system, because there is no physical connection point between the adjacent TSs of RSDE. Thus, it is also necessary to study the RSDE topology for both the DCAT system and the existing system verifications. Furthermore, Wang *et al.* [23] focus on the rail potential of train, but more attention should be paid to the rail potential of TS which is related to the safety of passengers and equipment.

Therefore, this article discussed the dynamic performance analysis and optimization of the DCAT system in detail and proposed the new topology of RSDE for both the DCAT system and the existing system verifications. Meanwhile, the dynamic performance index (DPI) is introduced to evaluate the rail potential and stray current mitigation of the DCAT system, and the optimization of the DCAT system is developed with DPI. Here, DPI is defined as the rail potential and stray current ratios of the DCAT system to the existing system, which may predict the dynamic performance of the DCAT system based on the observed rail potential and stray current of the existing system in URT.

The rest article is organized as follows. First, the typical configurations and operation principles of the DCAT system

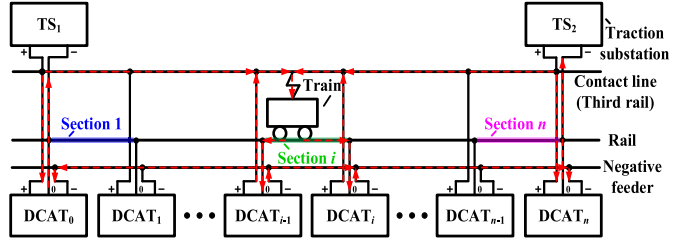


Fig. 2. Typical configuration of the DCAT system.

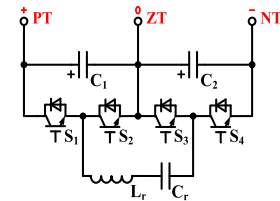


Fig. 3. Configuration of DCAT.

and RSDE are presented in Section II. Then, the dynamic performance analysis and optimization of the DCAT system with the proposed DPI are discussed in Section III. Moreover, Section IV shows the simulation results and verifies the theoretical analysis with the actual dynamic characteristics of URT, while the experimental verification are obtained in Section V based on the hardware platforms of the DCAT system and RSDE. Finally, the conclusions of this article are given in Section VI.

## II. DCAT SYSTEM AND RSDE

### A. DCAT System

Fig. 2 shows the typical configuration of the DCAT system, which adds the negative feeder and several DCATs compared with the existing system [23]. Here, the running rail is divided into  $n$  sections with  $n + 1$  DCATs (i.e.,  $\text{DCAT}_0$ – $\text{DCAT}_n$ ), and the current distribution when the train is running on section  $i$  is shown as Fig. 2. Obviously, the rail current of the DCAT system only exists in section  $i$  (i.e., train-running section), and the rail currents of other sections (i.e., no-train sections) are zero. Therefore, the DCAT system may solve the rail potential and stray current issues fundamentally.

As shown in Fig. 3, DCAT consists of two dc-link capacitors  $C_1$  and  $C_2$ , four switches  $S_1$ – $S_4$ , and one resonant unit (i.e., resonant inductor  $L_r$  and resonant capacitor  $C_r$ ). The positive terminal (PT), zero terminal (ZT), and negative terminal (NT) of DCAT are connected to the contact line, rail, and negative feeder, respectively. Moreover, the switches and resonant unit realize bidirectional energy transfer between dc-link capacitors, which can be divided into the boost mode (i.e.,  $C_1$  transfers the energy to  $C_2$ ) and the buck mode (i.e.,  $C_2$  transfers the energy to  $C_1$ ), and then ensure the voltage balance of dc-link capacitors. For the DCAT system as shown in Fig. 2,  $\text{DCAT}_0$  and  $\text{DCAT}_n$  operate in the boost mode, and  $\text{DCAT}_{i-1}$  and  $\text{DCAT}_i$  operate in the buck mode, while other DCATs have no energy flow.

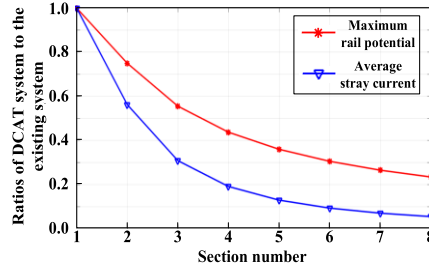


Fig. 4. Rail potential and stray current ratios of the DCAT system to the existing system.

Rail potential and stray current may be affected by different grounding schemes [31], [32], and URT prefers the floating scheme to reduce the stray current [15]. Therefore, based on the floating scheme, Wang *et al.* [23] show that the maximum rail potential and average stray current of the DCAT system are reduced to  $(2n - 1)/n^2$  and  $(2n - 1)^2/n^4$  as shown in Fig. 4 compared with the existing system; here, the rail is divided into  $n$  sections equally. Obviously, with the increase in the section number  $n$ , the rail potential and stray current mitigation performance of the DCAT system will be better, but the cost will be increased. Therefore, with comprehensive consideration of cost and performance, the recommended section number of DCAT system is 3–5 under different distances between adjacent TSs.

### B. RSDE

To obtain the rail potential and stray current behavior of URT, the field test may be the most direct and effective solution. But it is very costly, difficult, unsafe, and impractical to test the new traction power supply system on URT. RSDE is one of the general solutions for experimental verification [30], which can simulate the dynamic characteristics of the train position and current changing in the laboratory. However, the traditional RSDE in [30] cannot provide the physical connection point on contact line and rail for DCAT integration, and thus the new RSDE as shown in Fig. 5 is proposed in this article.

Taking the three-section RSDE as an example, RSDE mainly consists of three rail units (RUs), three contact line units (CUs), and one train unit (TU) as shown in Fig. 5. RU and CU may adopt the fixed resistor to describe the rail/contact line resistance and rail-to-earth resistance, while TU is built on the electronic variable resistance (EVR) for simulating the train position moving within a certain range. The switching states of RSDE are listed in Table I. Obviously, TU is always used as the train-running section, while RU and CU act as the no-train sections or be bypassed according to the train position.

Fig. 6 shows the configuration of TU. Here, EVR of TU can be divided into two types based on the range of resistance, that is, the electronic variable low-resistance (EVLR) and electronic variable high-resistance (EVHR). Here, EVLR and EVHR are used to simulate the rail/contact line resistance and rail-to-earth resistance, respectively. The operation modes of

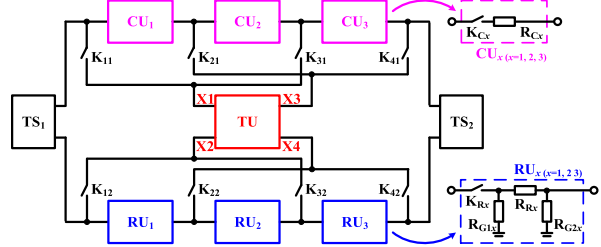


Fig. 5. RSDE configuration.

TABLE I  
SWITCHING STATES OF RSDE

Train is running on	K <sub>11,12</sub>	K <sub>21,22</sub>	K <sub>31,32</sub>	K <sub>41,42</sub>	K <sub>C1,R1</sub>	K <sub>C2,R2</sub>	K <sub>C3,R3</sub>
Section 1	ON	ON	OFF	OFF	OFF	ON	ON
Section 2	OFF	ON	ON	OFF	ON	OFF	ON
Section 3	OFF	OFF	ON	ON	ON	ON	OFF

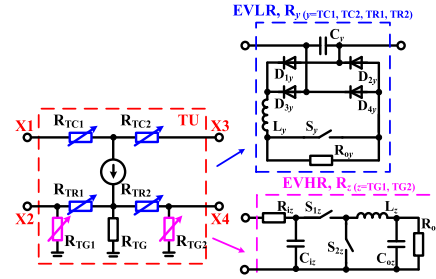


Fig. 6. TU configuration.

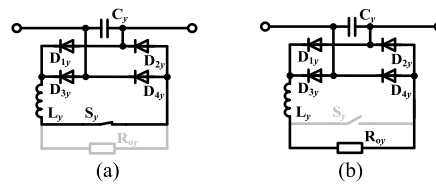


Fig. 7. Operation modes of EVLR. (a) Mode a. (b) Mode b.

EVLR (i.e.,  $R_{y,y} = TC1, TC2, TR1, TR2$ ) are as shown in Fig. 7, and the equivalent resistance  $R_y$  can be changed by controlling the duty ratio of switch  $S_y$ . Obviously, when the switch  $S_y$  is turned on as shown in Fig. 7(a), the equivalent resistance is zero; while the switch  $S_y$  is turned off as shown in Fig. 7(b), the equivalent resistance is  $R_{oy}$ . Thus, the relationship between the equivalent resistance  $R_y$  and the duty ratio  $D_{Sy}$  of switch  $S_y$  is calculated as follows, and the adjustable resistance range of  $R_y$  is  $[0, R_{oy}]$

$$R_y = (1 - D_{Sy})R_{oy}. \quad (1)$$

The operation modes of EVHR (i.e.,  $R_{z,z} = TG1, TG2$ ) are shown in Fig. 8. When the switch  $S_{1z}$  is turned on and  $S_{2z}$  is turned off as shown in Fig. 8(a), the equivalent resistance is  $R_{iz} + R_{oz}$ ; when the switch  $S_{1z}$  is turned off and  $S_{2z}$  is turned on as shown in Fig. 8(b), the equivalent resistance is infinite. Thus, the relationship between the equivalent resistance  $R_z$

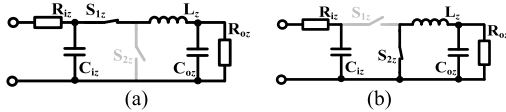


Fig. 8. Operation modes of EVHR. (a) Mode a. (b) Mode b.

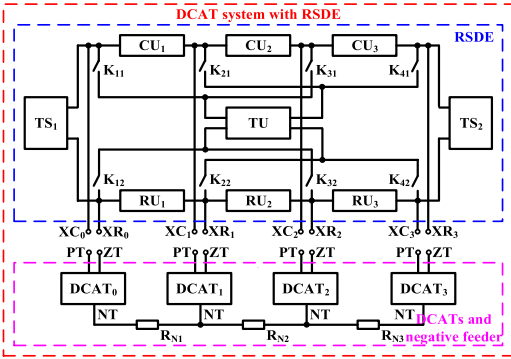


Fig. 9. Electrical connection of the DCAT system with RSDE.

and the duty ratio  $D_{S1z}$  may also be derived as follows, and the adjustable resistance range of  $R_z$  is  $[R_{iz} + R_{oz}, +\infty)$

$$R_z = R_{iz} + \frac{R_{oz}}{D_{S1z}^2}. \quad (2)$$

Meanwhile, it should be noted that all the resistors of  $RU_x$  and  $CU_{x(x=1,2,3)}$ , and  $R_{TG}$  of TU are related to the corresponding section length. When the section length is fixed, the traditional resistor can be used for RSDE for reducing cost and simplifying control. Furthermore, EVLR and EVHR can also be adopted to replace the traditional resistors in RU, CU, and TU. Then there is no need to replace the traditional resistor with other values, and there is only need to adjust the switch duty cycles of EVLR and EVHR, when the length of each section changes according to DCAT position adjustment. Therefore, the proposed RSDE may simulate the rail potential and stray current of the existing system directly, which can also be used to obtain the rail potential and stray current of the DCAT system as shown in Fig. 9 after connecting with DCATs and negative feeder. Here, the terminals  $XC_m$  and  $XR_{m(m=0,1,2,3)}$  of RSDE are connected with PT and ZT of  $DCAT_m$ , respectively.

### III. DYNAMIC PERFORMANCE ANALYSIS AND OPTIMIZATION

Taking the three-section DCAT system as an example, the equivalent models of the existing system and DCAT system are as shown in Fig. 10. The following assumptions are adopted for simplifying the analysis.

- 1)  $TS_1$  and  $TS_2$  are equivalent to the voltage sources  $V_s$ , and the train is equivalent to the current source  $I_o$ .
- 2) Rail resistance is  $R$ , while the contact line resistance and negative feeder resistance are  $M \cdot R$ ; here,  $M$  is the resistance ratio.
- 3) Rail-to-earth resistance  $R_g$  is large enough to ensure that the leaked current is much less than the rail current.

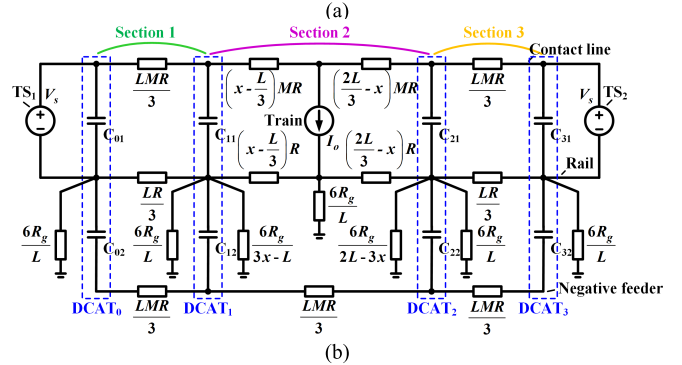
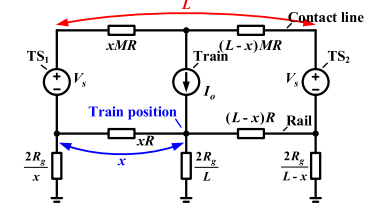


Fig. 10. Equivalent model configurations. (a) Existing system. (b) DCAT system when the train is running on section 2.

- 4) The distance between  $TS_1$  and  $TS_2$  is  $L$ , and the distance between the train and  $TS_1$  is  $x$ .
- 5) The rail is divided into three sections equally with  $DCAT_0$ - $DCAT_3$ .

However, the effects of the DCAT system on the rail potential and stray current mitigation are not easily obtained because it may change with different railway lines and train operating conditions. It is necessary to eliminate the influence of changing train current with the introduced DPI. Here, define DPI as the ratio  $K = X_D/X_e$ , where  $X_D$  and  $X_e$  are the rail potential or stray current of DCAT system and the existing system, respectively, then DPI is independent of the train current because of the division  $K = X_D/X_e$ . Therefore, DPI (i.e., the rail potential and stray current ratios) may show the potential in quantifying the dynamic performance of the DCAT system.

#### A. Rail Potential Ratio of Train

Based on the equivalent models as shown in Fig. 10, for the existing system, the rail potential of train  $V_{et}$  is derived as

$$V_{et} = \frac{(L-x)xRI_o}{2L}, \quad 0 \leq x \leq L. \quad (3)$$

For the DCAT system, considering that the rail-to-earth currents are equal to the earth-to-rail currents, the rail potential of train  $V_{Dt}$  is given as

$$V_{Dt} = \frac{5(x - \frac{i-1}{3}L)(\frac{i}{3}L - x)RI_o}{2L}, \quad \frac{i-1}{3}L \leq x < \frac{i}{3}L \quad (4)$$

where the train is running on section  $i$  ( $i = 1, 2, 3$ ). Based on (3) and (4), the rail potential ratio of train  $K_{rpt}$  is obtained as

$$K_{rpt} = \frac{V_{Dt}}{V_{et}} = \frac{5(x - \frac{i-1}{3}L)(\frac{i}{3}L - x)}{(L-x)x}, \quad \frac{i-1}{3}L \leq x < \frac{i}{3}L. \quad (5)$$

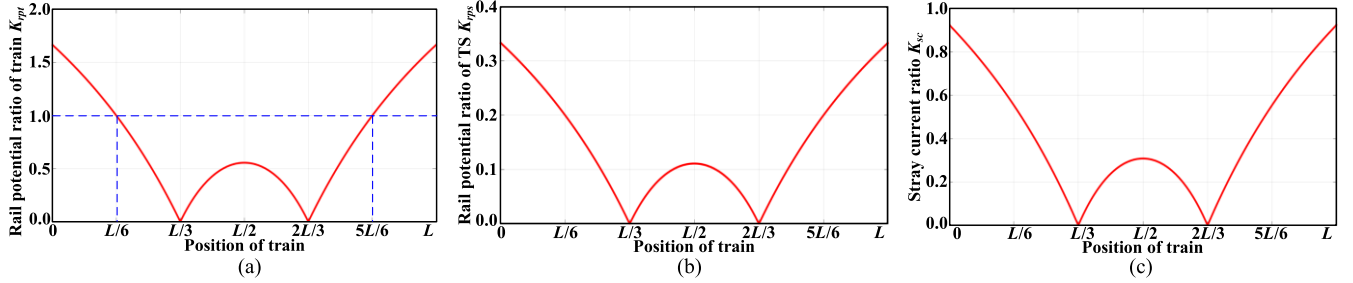


Fig. 11. Rail potential and stray current ratios of the DCAT system to the existing system. (a) Rail potential ratio of train  $K_{rpt}$ . (b) Rail potential ratio of TS  $K_{rps}$ . (c) Stray current ratio  $K_{sc}$ .

### B. Rail Potential Ratio of TS

For the existing system or the DCAT system, the rail potential of  $TS_1$  and  $TS_2$  is equal. Considering that the rail potential of TS and train is ideally equal and opposite, the rail potential of TS  $V_{es}$  of the existing system is described as

$$V_{es} = -\frac{(L-x)xRI_o}{2L}, \quad 0 \leq x \leq L. \quad (6)$$

Furthermore, the rail potential of TS  $V_{Ds}$  of the DCAT system is calculated as

$$V_{Ds} = -\frac{(x - \frac{i-1}{3}L)(\frac{i}{3}L - x)RI_o}{2L}, \quad \frac{i-1}{3}L \leq x < \frac{i}{3}L. \quad (7)$$

Thus, based on (6) and (7), the rail potential ratio of TS  $K_{rps}$  is given as

$$K_{rps} = \frac{V_{Ds}}{V_{es}} = \frac{(x - \frac{i-1}{3}L)(\frac{i}{3}L - x)}{(L-x)x}, \quad \frac{i-1}{3}L \leq x < \frac{i}{3}L. \quad (8)$$

### C. Stray Current Ratio

Stray current is the total rail-to-earth leaked currents, which equals to the total earth-to-rail feedback currents based on Kirchhoff's current law. Then, the stray current of the existing system  $I_e$  and DCAT system  $I_D$  is described as

$$I_e = \frac{(L-x)xRI_o}{8R_g}, \quad 0 \leq x \leq L \quad (9)$$

$$I_D = \frac{25(x - \frac{i-1}{3}L)(\frac{i}{3}L - x)RI_o}{72R_g}, \quad \frac{i-1}{3}L \leq x < \frac{i}{3}L. \quad (10)$$

Based on (9) and (10), the stray current ratio  $K_{sc}$  is derived as

$$K_{sc} = \frac{I_D}{I_e} = \frac{25}{9} \frac{(x - \frac{i-1}{3}L)(\frac{i}{3}L - x)}{(L-x)x}, \quad \frac{i-1}{3}L \leq x < \frac{i}{3}L. \quad (11)$$

### D. Analysis of DPI

Based on (5), (8), and (11), the DPI of the three-section DCAT system is shown in Fig. 11, which show the performances of the DCAT system when the train is running from  $TS_1$  to  $TS_2$ , no matter what the value and direction of the train current are. Compared with the existing system, the DCAT

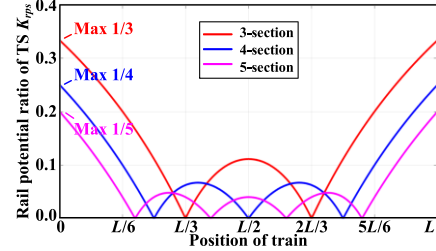


Fig. 12. Rail potential ratio of TS  $K_{rps}$  under different sections.

system reduces the rail potential or stray current when DPI is less than 1, while it increases the rail potential or stray current when DPI is greater than 1. Obviously, the smaller the DPI, the better the mitigation performance of the DCAT system.

As shown in Fig. 11(a), the rail potential ratio of the train is greater than 1 on sections  $[0, L/6]$  and  $[5L/6, L]$ , which means that the rail potential of the train in the DCAT system is higher than that in the existing system when the train is running on sections  $[0, L/6]$  and  $[5L/6, L]$ . Meanwhile, the rail potential ratio of TS as shown in Fig. 11(b) shows better performance than that of the train. Here, the rail potential ratio of TS is always smaller than 0.4, which means that the DCAT system guarantees the safety of passengers and equipment more effectively. Fig. 11(c) shows that the stray current ratio is always smaller than 1. Furthermore, DPI is generally smaller on section 2 (i.e.,  $[L/3, 2L/3]$ ) than that of section 1 (i.e.,  $[0, L/3]$ ) and section 3 (i.e.,  $[2L/3, L]$ ), which means that the DCAT system has the better rail potential and stray current mitigation performance on section 2.

Therefore, the dynamic performance of the DCAT system in any URT can be obtained with DPI. For example, the rail potential of the train in the DCAT system can be calculated from multiplying ratio  $K_{rpt}$  with the actual rail potential of the train in the existing system, no matter the value and direction of train current.

Moreover, for the  $n$ -section DCAT system, DPI can be described as

$$\begin{cases} K_{rpt} = (2n-1)\lambda_n \\ K_{rps} = \lambda_n \\ K_{sc} = \frac{(2n-1)^2}{n^2}\lambda_n \end{cases} \quad (12)$$

$$\lambda_n = \frac{(x - \frac{i-1}{n}L)(\frac{i}{n}L - x)}{(L-x)x}, \quad \frac{i-1}{n}L \leq x < \frac{i}{n}L \quad (13)$$

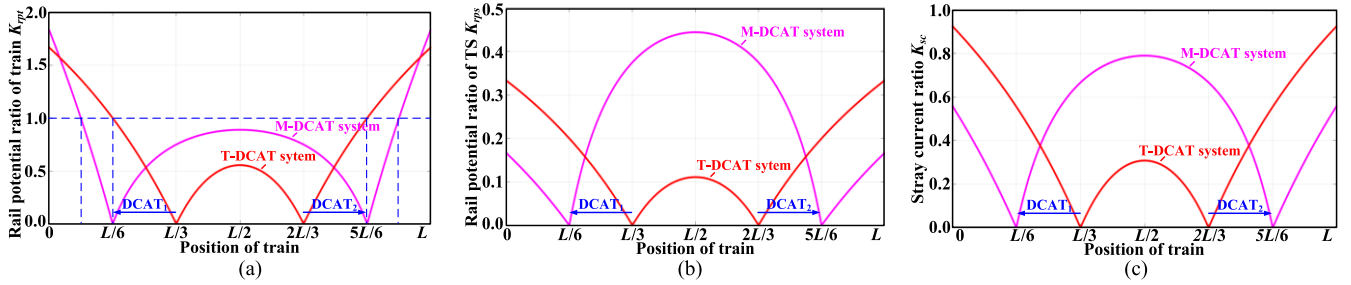


Fig. 13. DPI comparisons between M-DCAT system and T-DCAT system. (a) Rail potential ratio of train  $K_{rpt}$ . (b) Rail potential ratio of TS  $K_{rps}$ . (c) Stray current ratio  $K_{sc}$ .

where the train is running on section  $i = 1, 2, \dots, n$ .  $\lambda_n$  is defined as the basic ratio of  $n$ -section DCAT system's DPI. Taking the rail potential of TS as an example, the ratio  $K_{rps}$  under different sections is as shown in Fig. 12. Obviously, with the increase in the number of sections  $n$ , the maximum of  $K_{rps}$  is reduced to  $1/n$ , which means that the DCAT system shows better rail potential mitigation performance.

#### E. Optimization of DCAT System

The train current  $I_o$  is generally quite large under the traction and braking conditions. So the rail potential and stray current issues are particularly prominent when the train near TSs. However, Fig. 11 shows that DPI near TSs may be larger than that far away from TSs (i.e., the middle between TSs), and even the rail potential of the train increases slightly when the train is running on sections  $[0, L/6]$  and  $[5L/6, L]$ . Therefore, it is necessary to optimize the DCAT system to reduce DPI near TSs for better rail potential and stray current mitigation performance.

Fig. 12 shows that increasing the section number may reduce DPI near TSs, but the cost increases with more sections (i.e., more DCATs). So if keep the section number unchanged, optimizing DCAT system by adjusting the length of each section may reduce DPI, because the section length is directly related to the rail potential and stray current of the system. Then, the DPI of arbitrary length of each section can be derived as follows:

$$\left\{ \begin{array}{l} K_{rpt} = \frac{2L - \Delta X_i}{\Delta X_i} \lambda_X \\ K_{rps} = \lambda_X \end{array} \right. \quad \Delta X_i = X_i - X_{i-1} \quad (14)$$

$$\left\{ \begin{array}{l} K_{sc} = \frac{(2L - \Delta X_i)^2}{L^2} \lambda_X, \\ \lambda_X = \frac{(X_i - x)(x - X_{i-1})}{(L - x)x}, \quad X_{i-1} \leq x < X_i \end{array} \right. \quad (15)$$

where  $X_i$  and  $X_{i-1}$  are the positions of DCAT $_i$  and DCAT $_{i-1}$ , respectively (i.e., the distance between DCAT and TS $_1$ ), and  $\Delta X_i$  is the length of section  $i$  ( $i = 1, 2, \dots, n$ ). For  $n$ -section DCAT system, DCAT $_0$  and DCAT $_n$  are generally installed in TS $_1$  and TS $_2$ . Then adjusting the positions of DCAT $_1$ -DCAT $_{n-1}$  (i.e., other DCATs besides DCAT $_0$  and DCAT $_n$ ) may optimize the DCAT system and reduce DPI near TSs with high rail potential and stray current.

Taking the above three-section DCAT system as an example, for the traditional DCAT system (i.e., T-DCAT system), the rail is divided into three sections equally by installing DCAT $_0$  to

DCAT $_3$ ; here,  $X_0 = 0$ ,  $X_1 = L/3$ ,  $X_2 = 2L/3$ , and  $X_3 = L$ . for the moved DCAT system (i.e., M-DCAT system), shorten the lengths of section where the train is running under the traction and braking conditions (i.e., sections 1 and 3, respectively) for rail potential and stray current mitigation. Keeping DCAT $_0$  and DCAT $_3$  positions unchanged, DCAT $_1$  position changes from  $L/3$  to  $L/6$ , while DCAT $_2$  position changes from  $2L/3$  to  $5L/6$ . It should be clear that the above-mentioned DCAT position adjustment is just a simple case to distinguish with T-DCAT system; that is to say, the specific adjustment of the DCAT system should be discussed in combination with the actual URT and its train operating conditions.

Then DPI comparisons between M-DCAT system and T-DCAT system are shown in Fig. 13 through further derivation. Clearly, for the M-DCAT system, the DPI of sections  $[0, L/6]$  and  $[5L/6, L]$  is generally reduced at the cost of increasing DPI of section  $[L/6, 5L/6]$ . But the train is running on sections  $[0, L/6]$  and  $[5L/6, L]$  under the traction or braking condition with high current, while section  $[L/6, 5L/6]$  under the coasting condition with low current. Then the cost of increasing DPI on section  $[L/6, 5L/6]$  is almost negligible compared with reducing DPI of sections  $[0, L/6]$  and  $[5L/6, L]$ . Meanwhile, the M-DCAT system reduces the section length where the rail potential ratio of train  $K_{rpt}$  is greater than 1. Thus, the M-DCAT system reduces DPI near TSs with serious rail potential and stray current issues, which is more suitable for URT rail potential and stray current mitigation.

#### IV. SIMULATION RESULTS

To verify the above-mentioned theoretical analysis, the simulation models with dynamic characteristics of the existing system and DCAT system as shown in Fig. 2 were built. Beijing Subway Yizhuang Line is taken as an example to verify the dynamic performance of the DCAT system. The dynamic characteristics from Songjiazhuang Station (i.e., TS $_1$ ) to Xiaocun Station (i.e., TS $_2$ ) are shown in Fig. 14, and other simulation parameters are listed in Table II.

The rail potential and stray current comparisons between the simulation results and theoretical results are shown in Fig. 15, and the simulation results are listed in Table III. Here, the theoretical results of the existing system in the simulation are calculated based on the train current as shown in Fig. 14(a). Then the theoretical results of the DCAT system are obtained from the theoretical results of the existing system and DPI.

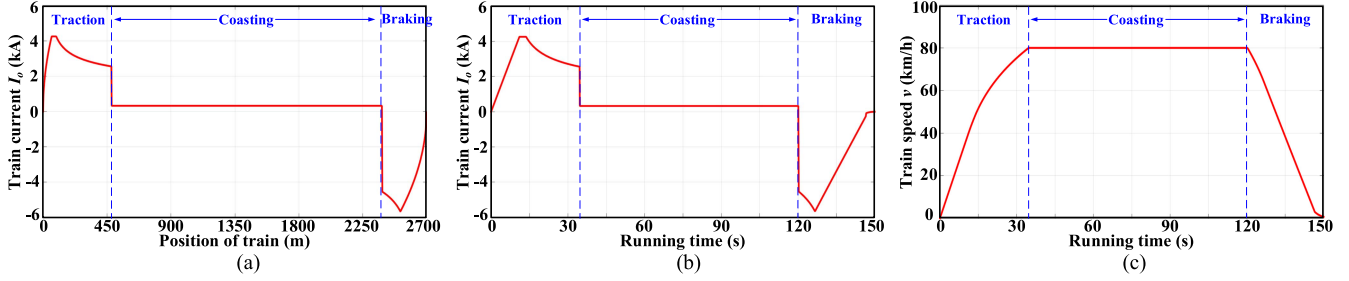


Fig. 14. Dynamic characteristics of Beijing Subway Yizhuang Line from Songjiangzhuang Station to Xiaocun Station. (a) Train current–position curve. (b) Train current–time curve. (c) Train speed–time curve.

TABLE II  
SIMULATION PARAMETERS

Variable	Description	Value	Variable	Description	Value
$V_s$	TS voltage	750V	$R_g$	Rail-to-earth resistance	$1.5\Omega\cdot\text{km}$
$L$	Distance between TSs	2.7km	$M$	Resistance ratio	3
$T$	Running time	150s	$n$	Number of sections	3
$R$	Rail resistance	$30\text{m}\Omega/\text{km}$			

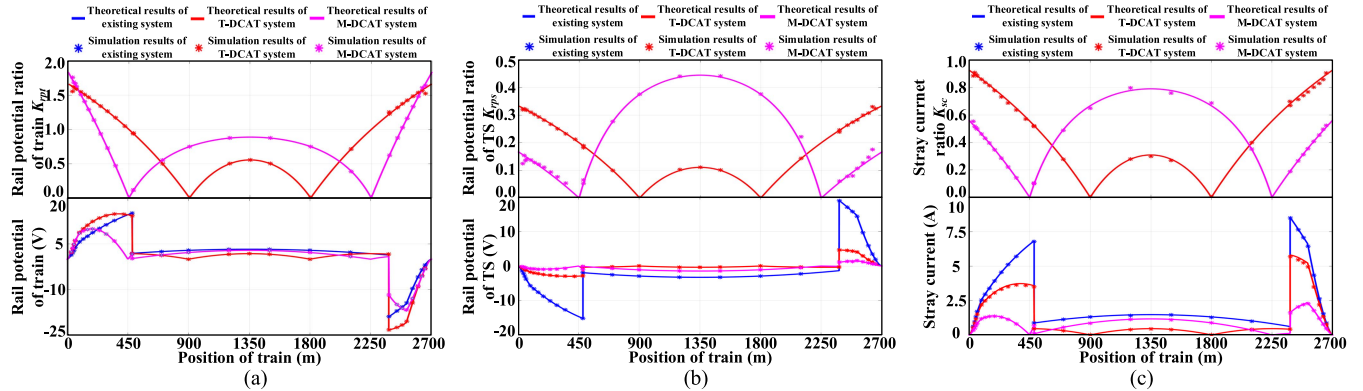


Fig. 15. Rail potential and stray current comparisons between the simulation results and theoretical results. (a) Rail potential of train. (b) Rail potential of TS. (c) Stray current.

TABLE III  
SIMULATION RESULTS

		Maximum of traction condition			Maximum of braking condition		
		Theoretical	Simulation	Error	Theoretical	Simulation	Error
Rail potential of train	Existing system	15.18V	15.15V	0.20%	18.96V	18.92V	0.21%
	T-DCAT system	14.91V	14.84V	0.34%	23.23V	23.26V	0.13%
	M-DCAT system	9.98V	9.95V	0.30%	17.00V	16.81V	1.11%
Rail potential of TS	Existing system	15.18V	15.16V	0.13%	18.96V	18.92V	0.21%
	T-DCAT system	2.98V	2.99V	0.33%	4.65V	4.65V	0.00%
	M-DCAT system	0.90V	0.91V	1.11%	1.54V	1.55V	0.65%
Stray current	Existing system	6.83A	6.78A	0.73%	8.53A	8.50A	0.35%
	T-DCAT system	3.73A	3.62A	2.95%	5.81A	5.68A	2.24%
	M-DCAT system	1.37A	1.36A	0.73%	2.34A	2.28A	2.56%

Fig. 15(a) shows the rail potential comparisons of train, and the rail potential changes little between the existing system and DCAT system (i.e., both T-DCAT system and M-DCAT

system). For the coasting condition, the rail potential ratio of train  $K_{rpt}$  is always less than 1. Considering the small train current of coasting condition, the rail potential of train

TABLE IV  
EXPERIMENTAL PARAMETERS OF T-DCAT SYSTEM

Variable	Description	Value	Variable	Description	Value
$V_s$	TS voltage	400V	$R_{TG}$	Rail-to-earth resistor of TU	$250\Omega$
$T$	Running time	10s	$R_{oy}$	Resistor of EVLR	$2.5\Omega$
$C$	DC-link capacitor of DCATs	$900\mu F$	$C_y$	Capacitor of EVLR	$650\mu F$
$C_r$	Resonant capacitor of DCATs	$50\mu F$	$L_y$	DC inductor of EVLR	$500\mu H$
$L_r$	Resonant inductor of DCATs	$20\mu H$	$R_{iz}$	Input resistor of EVHR	$50\Omega$
$f_{s\_DCAT}$	Switching frequency of DCATs	5kHz	$R_{oz}$	Output resistor of EVHR	$200\Omega$
$R_{Cx}$	Contact line resistor of CUs	$2.5\Omega$	$L_z$	DC inductor of EVHR	$500\mu H$
$R_{Rx}$	Rail resistor of RUs	$2.5\Omega$	$C_{iz}$	Input capacitor of EVHR	$22\mu F$
$R_{G1x}, R_{G2x}$	Rail-to-earth resistor of RUs	$250\Omega$	$C_{oz}$	Output capacitor of EVHR	$4.7\mu F$

is negligible compared with that of traction and braking conditions, then the rail potential mitigation of the DCAT system may be insignificant. Meanwhile, for the traction and braking conditions, the ratio  $K_{rpt}$  is generally larger than 1, and thus DCAT system may increase the rail potential of train. For the T-DCAT system, the maximum rail potential of traction condition reduces to 97.95%, while the maximum of braking condition increases to 122.94% as shown in Table III. Although the maximum of traction condition decreases slightly, the rail potential of the T-DCAT system is larger than that of the existing system under most traction and braking conditions, which is clearly contrary to the expected rail potential mitigation. Compared with the T-DCAT system, the M-DCAT system may reduce the rail potential more effectively based on the theoretical analysis. For the M-DCAT system, the maximum rail potential of traction and braking conditions reduces to 65.68% and 88.85%, respectively, compared with the existing system. Therefore, the M-DCAT system may reduce the rail potential of train, especially for traction condition.

For the rail potential comparisons of TS as shown in Fig. 15(b), the rail potential is significantly reduced with the DCAT system. Here, the rail potential ratio of TS  $K_{rps}$  is always less than 0.5 for both the T-DCAT system and M-DCAT system, which proves the effectiveness of the DCAT system on rail potential mitigation. The ratio  $K_{rps}$  of the M-DCAT system decreases under traction and braking conditions, while it increases under coasting condition compared with the T-DCAT system. The rail potential of TS is equal and opposite with that of the train in the existing system, while the rail potential of TS is generally lower than that of the train in the DCAT system. For the T-DCAT system, the maximum rail potential of traction condition reduces to 19.72% as shown in Table III, while the maximum of braking condition reduces to 24.57% compared with the existing system. The rail potential of TS can be further reduced with the M-DCAT system, and the maximums of traction and braking conditions reduce to 6.00% and 8.19% compared with the existing system. Therefore, DCAT system shows better mitigation performance on the rail potential of TS compared

with the rail potential of train, which ensures personal safety and lowers the activated frequency of OVPD effectively.

The stray current comparisons are shown in Fig. 15(c), and the stray current of system is also suppressed, especially in M-DCAT system. The stray current ratio  $K_{sc}$  is always less than 1, which also proves the effectiveness of DCAT system on stray current mitigation. Similar to the rail potential ratio of TS  $K_{rps}$ , the ratio  $K_{sc}$  of M-DCAT system also decreases under the traction and braking conditions and increases under the coasting condition compared with the T-DCAT system. For the T-DCAT system, the maximum stray currents of traction and braking conditions reduce to 53.39% and 66.82% as shown in Table III, respectively, and the average stray current when the train runs from TS1 to TS2 reduces to 51.66% (i.e., from 2.11 to 1.09 A) compared with the existing system. For the M-DCAT system, the maximum stray currents of traction and braking conditions reduce to 20.06% and 26.82%, and the average stray current reduces to 39.81% (i.e., from 2.11 to 0.84 A). So the simulation results prove that M-DCAT system has better stray current mitigation performance compared with T-DCAT system.

Therefore, for the rail potential and stray current of the DCAT system and the existing system, the simulation results coincide with the theoretical results. The maximum error of rail potentials is about 1%, while the maximum error of stray currents is limited to 3%. Hence, the theoretical analysis is validated by the simulation results effectively.

## V. EXPERIMENTAL VERIFICATION

To further verify the feasibility of theoretical analysis and simulation results, the laboratory prototype of the three-section DCAT system with RSDE was built as shown in Fig. 16. The experimental parameters of the T-DCAT system are given in Table IV, and the main circuit of the DCAT system with RSDE is shown as Fig. 9. Meanwhile, for experimental test of M-DCAT system, RSDE should adjust the resistors to achieve DCAT position movement. Compared with the T-DCAT system, RSDE resistors of the M-DCAT system are shown in Table V. Here, the rail-to-earth resistor of TU  $R_{TG}$  adopts EVHR to replace the fixed resistor, and the equivalent

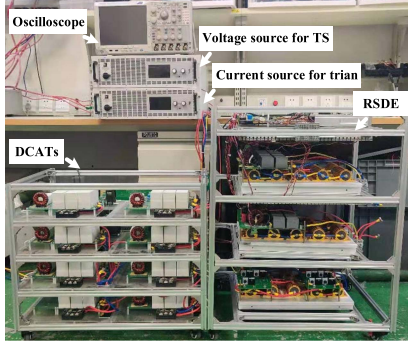


Fig. 16. Laboratory prototype of the three-section DCAT system with RSDE.

TABLE V  
RSDE RESISTORS COMPARISON BETWEEN T-DCAT SYSTEM AND M-DCAT SYSTEM

RSDE Resistors	Value of T-DCAT system	Value of M-DCAT system
$R_{C1}, R_{C3}, R_{R1}, R_{R3}$	2.5Ω	1.25Ω
$R_{C2}, R_{R2}$	2.5Ω	5Ω
$R_{G11}, R_{G21}, R_{G13}, R_{G23}$	250Ω	500Ω
$R_{G12}, R_{G22}$	250Ω	125Ω
$R_{oy}$	2.5Ω	5Ω
$R_{iz}$	50Ω	50Ω
$R_{oz}$	200Ω	75Ω

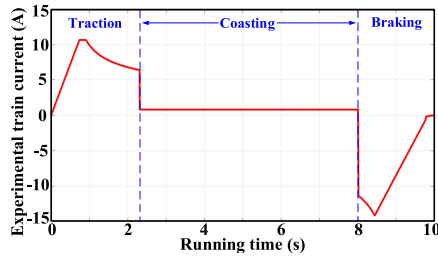


Fig. 17. Experimental train current curve.

resistance  $R_{TG}$  is 500, 125, and 500 Ω, respectively, when the train is running on sections 1–3.

Meanwhile, considering that the rail potentials of TSs are equal, the laboratory prototype as shown in Fig. 16 adopts one programmable bidirectional voltage source to simulate the TSs and uses another programmable bidirectional current source to simulate the train. Here, the experimental train current is shown as Fig. 17. Compared with the dynamic characteristics as shown in Fig. 14(b), the train current and running time are reduced to 1/400 and 1/15 of original for the convenience of experimental test. Furthermore, in the actual URT, the stray currents are hard to be observed directly, which are mainly derived by observing the rail potentials. Therefore, the experiments also mainly focus on the verification of rail potentials.

Fig. 18 shows the rail potentials of the existing system and DCAT system. Obviously, the experimental waveforms are basically similar to the theoretical results as shown in Fig. 15. The theoretical results are the curves changing with the position of train, while the experimental waveforms change with running time. For the existing system as shown in Fig. 18(a), the rail potentials of train and TS are equal and opposite, and the maximum rail potentials of traction and braking conditions are 3.8 and 4.1 V, respectively. For T-DCAT system as shown in Fig. 18(b), the maximum train rail potential of traction condition is equal to that of the existing system, but the rail potential of train may be larger at most traction condition. Similarly for braking condition, the maximum train rail potential increases slightly to 4.7 V. Meanwhile, the rail potential of TS decreases significantly. The maximum TS rail potentials of traction and braking conditions are reduced to 0.9 and 1.1 V (i.e., 23.68% and 26.83%) as shown in Table VI. Thus, T-DCAT system may reduce the rail potential of TS effectively, but the rail potential of train does not achieve the expected mitigation, even increases slightly. Moreover, for M-DCAT system as shown in Fig. 18(c), the maximum train rail potentials of traction and braking conditions are reduced to 2.7 and 3.8 V (i.e., 73.68% and 92.68%), while the maximum TS rail potentials of traction and braking conditions are reduced to 0.5 and 0.4 V (i.e., 13.16% and 7.32%) as shown in Table VI. Therefore, M-DCAT system may reduce the rail potential issue more effectively compared with T-DCAT system.

Meanwhile, based on the rail potential experimental results and relationship between stray current and rail potential, the experimental stray current waveforms are obtained as shown in Fig. 19. Obviously, for the existing system, the maximum stray currents of both traction and braking conditions are 22.8mA. With T-DCAT system, the maximum stray currents of traction and braking conditions reduce to 12.8 and 15.8 mA (i.e., 56.14% and 69.30%) as shown in Table VI, which shows the effectiveness of DCAT system on stray current mitigation. The stray current may be further reduced with the proposed M-DCAT system; here, the maximum stray current of traction and braking conditions reduce to 5.2 and 7.0 mA (i.e., 22.81% and 30.70%) as shown in Table VI. Thus, M-DCAT system also has a better performance on stray current suppression.

Meanwhile, according to DPI comparisons in Table VI, the experimental DPI is slightly larger than the theoretical DPI. On one hand, the experimental results always contain errors, especially when the tested voltage or current is very small while the measurement accuracy is not high enough; on the other hand, each DCAT may have a small voltage difference between two dc-link capacitors, which leads to rail current on no-train sections and increases the rail potential and stray current of the DCAT system. The voltage difference is generally limited to a very small range in the experiment, which may introduce error compared with the theoretical results. So experimental DPI is generally slightly larger than that of theory.

In conclusion, the experimental results have a good agreement with the theoretical results. The correctness and effectiveness of the theories and simulation analysis are validated by

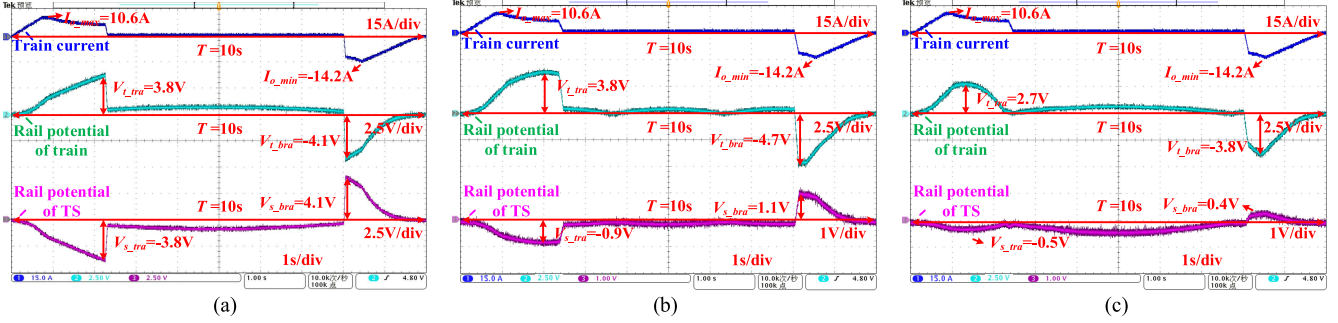


Fig. 18. Experimental results of rail potentials. (a) Existing system. (b) T-DCAT system. (c) M-DCAT system.

TABLE VI  
EXPERIMENTAL RESULTS

	Existing system	T-DCAT system	M-DCAT system	Experimental DPI of T-DCAT system	Theoretical DPI of T-DCAT system	Experimental DPI of M-DCAT system	Theoretical DPI of M-DCAT system
Maximum train rail potential of traction condition	3.8V	3.8V	2.7V	100.00%	98.22%	71.05%	65.74%
Maximum TS rail potential of traction condition	3.8V	0.9V	0.5V	23.68%	19.63%	13.15%	5.93%
Maximum stray current of traction condition	22.8mA	12.8mA	5.2mA	56.14%	54.57%	22.81%	20.10%
Maximum train rail potential of braking condition	4.1V	4.7V	3.8V	114.63%	122.52%	92.68%	89.66%
Maximum TS rail potential of braking condition	4.1V	1.1V	0.4V	26.83%	24.53%	9.76%	8.12%
Maximum stray current of braking condition	22.8mA	15.8mA	7.0mA	69.30%	68.07%	30.70%	27.41%

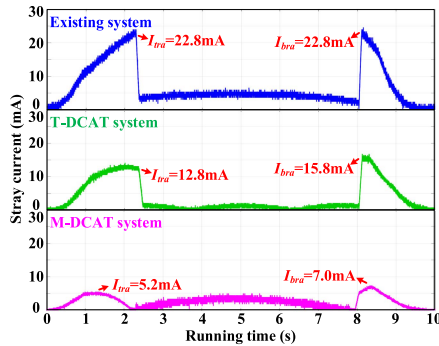


Fig. 19. Experimental results of stray currents.

the experimental results. Comparing the rail potential and stray current between the DCAT system and the existing system, the DCAT system solves the rail potential and stray current issues effectively, and the proposed M-DCAT system has better performances on rail potential and stray current mitigation compared with the T-DCAT system.

## VI. CONCLUSION

This article presented the dynamic performance analysis and optimization of DCAT system, and RSDE for both the DCAT system and the existing system verification is proposed.

Considering that the train dynamic performance changes with different URT, DPI is introduced to analyze the dynamic performance of DCAT system with wide applicability. Here, DPI mainly consists of rail potential and stray current ratios, which may predict the dynamic performances of DCAT system accurately based on the observed rail potential and stray current of the existing system. Meanwhile, the optimization of DCAT system is developed with DPI, and then M-DCAT system is proposed for better rail potential and stray current mitigation performance. Finally, the correctness and effectiveness of the theoretical analysis are validated through the simulation and experimental studies based on the dynamic characteristics of Beijing Subway Yizhuang Line. The results show that DCAT system, especially M-DCAT system, may solve the rail potential and stray current issues effectively, which leads to promising application prospect in URT.

## REFERENCES

- [1] Q. Gu, T. Tang, F. Cao, and Y.-D. Song, "Energy-efficient train operation in urban rail transit using real-time traffic information," *IEEE Trans. Intell. Transp. Syst.*, vol. 15, no. 3, pp. 1216–1233, Jun. 2014.
- [2] Y.-S. Tzeng and C.-H. Lee, "Analysis of rail potential and stray currents in a direct-current transit system," *IEEE Trans. Power Del.*, vol. 25, no. 3, pp. 1516–1525, Jul. 2010.
- [3] I. Cotton, C. Charalambous, P. Aylott, and P. Ernst, "Stray current control in DC mass transit systems," *IEEE Trans. Veh. Technol.*, vol. 54, no. 2, pp. 722–730, Mar. 2005.

- [4] A. Ogunsola, A. Mariscotti, and L. Sandrolini, "Estimation of stray current from a DC-electrified railway and impressed potential on a buried pipe," *IEEE Trans. Power Del.*, vol. 27, no. 4, pp. 2238–2246, Oct. 2012.
- [5] C. L. Pires, "What the IEC tells us about stray currents: Guidance for a practical approach," *IEEE Electrific. Mag.*, vol. 4, no. 3, pp. 23–29, Sep. 2016.
- [6] A. Dolara, F. Foiadelli, and S. Leva, "Stray current effects mitigation in subway tunnels," *IEEE Trans. Power Del.*, vol. 27, no. 4, pp. 2304–2311, Oct. 2012.
- [7] C. A. Charalambous, P. Aylott, and D. Buxton, "Stray current calculation and monitoring in DC mass-transit systems: Interpreting calculations for real-life conditions and determining appropriate safety margins," *IEEE Veh. Technol. Mag.*, vol. 11, no. 2, pp. 24–31, Jun. 2016.
- [8] S. Lin, Y. Huangfu, Q. Zhou, and A. Wang, "Evaluation and analysis model of stray current in the metro depot," *IEEE Trans. Transport. Electricif.*, early access, Nov. 3, 2020, doi: [10.1109/TTE.2020.3035395](https://doi.org/10.1109/TTE.2020.3035395).
- [9] S.-L. Chen, S.-C. Hsu, C.-T. Tseng, K.-H. Yan, H.-Y. Chou, and T.-M. Too, "Analysis of rail potential and stray current for Taipei Metro," *IEEE Trans. Veh. Technol.*, vol. 55, no. 1, pp. 67–75, Jan. 2006.
- [10] S. Kimura, T. Miyauchi, K. Oguma, H. Takahashi, and K. Teramura, "Rail potential calculation model for DC railway power supply equipped with voltage limiting device," in *Proc. 22nd Eur. Conf. Power Electron. Appl. (EPE ECCE Europe)*, Sep. 2020, pp. 1–9.
- [11] S. A. Memon and P. Fromme, "Stray current corrosion and mitigation: A synopsis of the technical methods used in DC transit systems," *IEEE Electrific. Mag.*, vol. 2, no. 3, pp. 22–31, Sep. 2014.
- [12] D. Paul, "DC stray current in rail transit systems and cathodic protection," *IEEE Ind. Appl. Mag.*, vol. 22, no. 1, pp. 8–13, Jan./Feb. 2016.
- [13] A. Zaboli, B. Vahidi, S. Yousefi, and M. M. Hosseini-Biyouki, "Evaluation and control of stray current in DC-electrified railway systems," *IEEE Trans. Veh. Technol.*, vol. 66, no. 2, pp. 974–980, Feb. 2017.
- [14] C. A. Charalambous, "Comprehensive modeling to allow informed calculation of DC traction systems' stray current levels," *IEEE Trans. Veh. Technol.*, vol. 66, no. 11, pp. 9667–9677, Nov. 2017.
- [15] S.-Y. Xu, W. Li, and Y.-Q. Wang, "Effects of vehicle running mode on rail potential and stray current in DC mass transit systems," *IEEE Trans. Veh. Technol.*, vol. 62, no. 8, pp. 3569–3580, Oct. 2013.
- [16] G. Du, J. Wang, X. Jiang, D. Zhang, L. Yang, and Y. Hu, "Evaluation of rail potential and stray current with dynamic traction networks in multitrain subway systems," *IEEE Trans. Transport. Electricif.*, vol. 6, no. 2, pp. 784–796, Jun. 2020.
- [17] Y. Wang, G. Zhang, R. Qiu, Z. Liu, and N. Yao, "Distribution correction model of urban rail return system considering rail skin effect," *IEEE Trans. Transport. Electricif.*, vol. 7, no. 2, pp. 883–891, Jun. 2021.
- [18] A. Mariscotti, "Electrical safety and stray current protection with platform screen doors in DC rapid transit," *IEEE Trans. Transport. Electricif.*, early access, Jan. 12, 2021, doi: [10.1109/TTE.2021.3051102](https://doi.org/10.1109/TTE.2021.3051102).
- [19] J. Fabre, P. Ladoux, E. Solano, G. Gateau, and J.-M. Blaqui  re, "MVDC three-wire supply systems for electric railways: Design and test of a full SiC multilevel chopper," *IEEE Trans. Ind. Appl.*, vol. 53, no. 6, pp. 5820–5830, Nov./Dec. 2017.
- [20] R. Fotouhi, S. Farshad, and S. S. Fazel, "A new novel DC booster circuit to reduce stray current and rail potential in DC railways," in *Proc. Compat. Power Electron.*, May 2009, pp. 457–462.
- [21] J. Gu, X. Yang, T. Q. Zheng, Z. Shang, Z. Zhao, and W. Guo, "Negative resistance converter traction power system for reducing rail potential and stray current in the urban rail transit," *IEEE Trans. Transport. Electricif.*, vol. 7, no. 1, pp. 225–239, Mar. 2021.
- [22] Z. Shang, X. Yang, J. Gu, and T. Q. Zheng, "Modeling of negative resistance converter traction power system," in *Proc. IEEE Energy Convers. Congr. Expo.*, Oct. 2020, pp. 6367–6371.
- [23] M. Wang, X. Yang, T. Q. Zheng, and M. Ni, "DC autotransformer-based traction power supply for urban transit rail potential and stray current mitigation," *IEEE Trans. Transport. Electricif.*, vol. 6, no. 2, pp. 762–773, Jun. 2020.
- [24] M. Wang, X. Yang, L. Wang, and T. Q. Zheng, "Resonant switched capacitor converter based DC auto-transformer for urban rail transit," in *Proc. IEEE Appl. Power Electron. Conf. Expo. (APEC)*, Mar. 2018, pp. 1441–1446.
- [25] M. Wang, X. Yang, T. Q. Zheng, and J. Gu, "The voltage difference control of DCAT traction power supply system for urban rail transit," in *Proc. IEEE Energy Convers. Congr. Expo. (ECCE)*, Sep. 2018, pp. 532–537.
- [26] Z. Yang, Z. Yang, H. Xia, and F. Lin, "Brake voltage following control of supercapacitor-based energy storage systems in metro considering train operation state," *IEEE Trans. Ind. Electron.*, vol. 65, no. 8, pp. 6751–6861, Aug. 2018.
- [27] X. Yang, X. Li, B. Ning, and T. Tang, "A survey on energy-efficient train operation for urban rail transit," *IEEE Trans. Intell. Transport. Syst.*, vol. 17, no. 1, pp. 2–13, Jul. 2016.
- [28] L. Zhao, J. Li, and M. Liu, "Simulation and analysis of metro stray current based on multi-locomotives condition," in *Proc. 35th Chin. Control Conf.*, Jul. 2016, pp. 9252–9258.
- [29] J. Tian, Y. Wang, G. Du, M. Fan, and J. Q. Hu, "Analysis of rail potential with the influence of multi-node power distribution in urban rail power supply system," in *Proc. 45th Annu. Conf. Ind. Electron. Soc.*, Oct. 2019, pp. 5444–5449.
- [30] A. Ibrahim, A. Elrayyah, Y. Sozer, and J. A. De Abreu-Garcia, "DC railway system emulator for stray current and touch voltage prediction," *IEEE Trans. Ind. Appl.*, vol. 53, no. 1, pp. 439–446, Jan./Feb. 2017.
- [31] C.-H. Lee and C.-J. Lu, "Assessment of grounding schemes on rail potential and stray currents in a DC transit system," *IEEE Trans. Power Del.*, vol. 21, no. 4, pp. 1941–1947, Oct. 2006.
- [32] M. M. Alamutti, H. Nouri, and S. Jamali, "Effects of earthing systems on stray current for corrosion and safety behaviour in practical metro systems," *IET Elect. Syst. Transp.*, vol. 1, no. 2, pp. 69–79, Apr. 2011.



**Miao Wang** (Student Member, IEEE) was born in Shandong, China, in 1994. He received the B.S. degree in electrical engineering from Beijing Jiaotong University, Beijing, China, in 2016, where he is currently pursuing the Ph.D. degree in power electronics with the School of Electrical Engineering.

His current research interests include dc–dc converters, multilevel converter, urban rail transit power supply, and stray current mitigation.



**Xiaofeng Yang** (Senior Member, IEEE) received the B.S. and Ph.D. degrees in electrical engineering from Beijing Jiaotong University, Beijing, China, in 2003 and 2011, respectively.

From 2003 to 2005, he was a Power Supplier Engineer with the Seventh Research Institute of China Ministry of Information Industry, Guangzhou, China. From 2012 to 2014, he was a Post-Doctoral Fellow with North Carolina State University, Raleigh, NC, USA. He is currently an Associate Professor with Beijing Jiaotong University. His current research interests include high-power energy converter, electrical energy router, and rail transit power supply.



**Menghan Ni** was born in Hebei, China, in 1995. He received the B.S. and M.S. degrees in electrical engineering from Beijing Jiaotong University, Beijing, China, in 2018 and 2021, respectively.

His current research interests include dc–dc converter, soft-switching technology, and urban rail transit power supply.



**Huikang Wang** was born in Shanxi, China, in 1996. He received the B.S. and M.S. degrees in electrical engineering from Beijing Jiaotong University, Beijing, China, in 2018 and 2021, respectively.

His current research interests include dc–dc converter application in stray current governance.



**Shixiang Li** was born in Henan, China, in 1995. He received the B.S. degree in electrical engineering from Henan Normal University, Xinxiang, China, in 2019. He is currently pursuing the M.S. degree in power electronics with the School of Electrical Engineering, Beijing Jiaotong University, Beijing, China.

His current research interests include dc–dc converter and urban rail transit power supply.



**Trillion Q. Zheng** (Senior Member, IEEE) received the B.S. degree in electrical engineering from Southwest Jiaotong University, Chengdu, China, in 1986, and the M.S. and Ph.D. degrees in electrical engineering from Beijing Jiaotong University, Beijing, China, in 1992 and 2002, respectively.

He is currently a Distinguished Professor with Beijing Jiaotong University. He is the Director of the Center for Electric Traction, founded by Ministry of Education, Beijing. His current research interests include the power supplies and ac drives of railway traction systems, high-performance and low-loss power electronics systems, photovoltaic (PV) converters and control, active power filters, and power quality correction.

Prof. Zheng received the Youth Award of Railway Science and Technology of Zhan Tianyou in 2005 and the Zhongda Scholar for power electronics and motor drive area by Delta Environmental and Educational Foundation in 2007.